nature energy

Article

https://doi.org/10.1038/s41560-024-01654-z

Electrochemical regeneration of high-purity CO_2 from (bi)carbonates in a porous solid electrolyte reactor for efficient carbon capture

Received: 31 May 2023

Accepted: 18 September 2024

Published online: 11 October 2024

Check for updates

Xiao Zhang [1,4] ✉, Zhiwei Fang [1,4], Peng Zhu [1,4], Yang Xia [1] & Haotian Wang [1,2,3] ✉

Carbon dioxide (CO_2) and absorbent regeneration are the most energy-intensive processes in carbon capture loops. Conventional carbon capture technologies typically consume substantial amounts of heat and involve multiple steps for regeneration. Here we demonstrated one-step electrochemical regeneration of CO_2 and alkaline absorbent from carbon-containing solutions in a modular porous solid electrolyte (PSE) reactor. By performing hydrogen evolution and oxidation redox reactions, our PSE reactor selectively split $NaHCO_3$/Na_2CO_3 solutions, which typically come from air contactors after CO_2 absorption, into NaOH absorbent in the catholyte and high-purity CO_2 gas in the PSE layer. No chemicals were consumed and no by-products were generated. High Na^+-ion transport number (~90%), high capture capacity retention (~90%), low energy consumptions (50 kJ mol_{CO2}^{-1} and 118 kJ mol_{CO2}^{-1} at 1 mA cm^{-2} and 100 mA cm^{-2} for bicarbonate, respectively) and long-term stability (>100 hours) were demonstrated. We achieved industrially relevant carbon regeneration rates of up to 1 A cm^{-2} (~18 mmol cm^{-2} h^{-1}), highlighting the promising application potential.

Before renewable energy can fully displace traditional fossil fuels in power industry, transportation and many other human activities, carbon capture from point sources or directly from the atmosphere, followed by either carbon sequestration or utilization, will remain as an effective tool to mitigate climate change[1–3]. As carbon dioxide (CO_2) is an acidic gas, one popular class of carbon capture technologies is based on the simultaneous neutralization reaction between low-concentration CO_2 and a basic solution (such as monoethanolamine or NaOH) to form carbon-containing products, followed by a regeneration process to produce high-concentration CO_2 while restoring the basic solution for the next round capture process[4,5]. This regeneration step, either thermally[3,5], chemically[5,6] or electrochemically[7–12], involves chemical bond dissociation to release CO_2 again and thus is usually the most energy- and cost-intensive step. For example, in the widely demonstrated amine-scrubbing carbon capture technologies, the CO_2 desorption process needs ~110 to 140 °C water vapour stripping and was estimated to account for ~70% of the overall operating cost[13,14].

Compared to the amine-based sorbents, basic aqueous solutions (such as NaOH or KOH) showed distinct advantages for large-scale carbon capture applications including low corrosion, high stability, high capture rates, no sensitivity to oxygen and environmental benignity[5,15]. However, due to its strong CO_2 absorption capability to form very stable

[1]Department of Chemical and Biomolecular Engineering, Rice University, Houston, TX, USA. [2]Department of Chemistry, Rice University, Houston, TX, USA. [3]Department of Materials Science and NanoEngineering, Rice University, Houston, TX, USA. [4]These authors contributed equally: Xiao Zhang, Zhiwei Fang, Peng Zhu. ✉e-mail: xiao1.zhang@polyu.edu.hk; htwang@rice.edu

https://doi.org/10.1038/s41560-024-01654-z

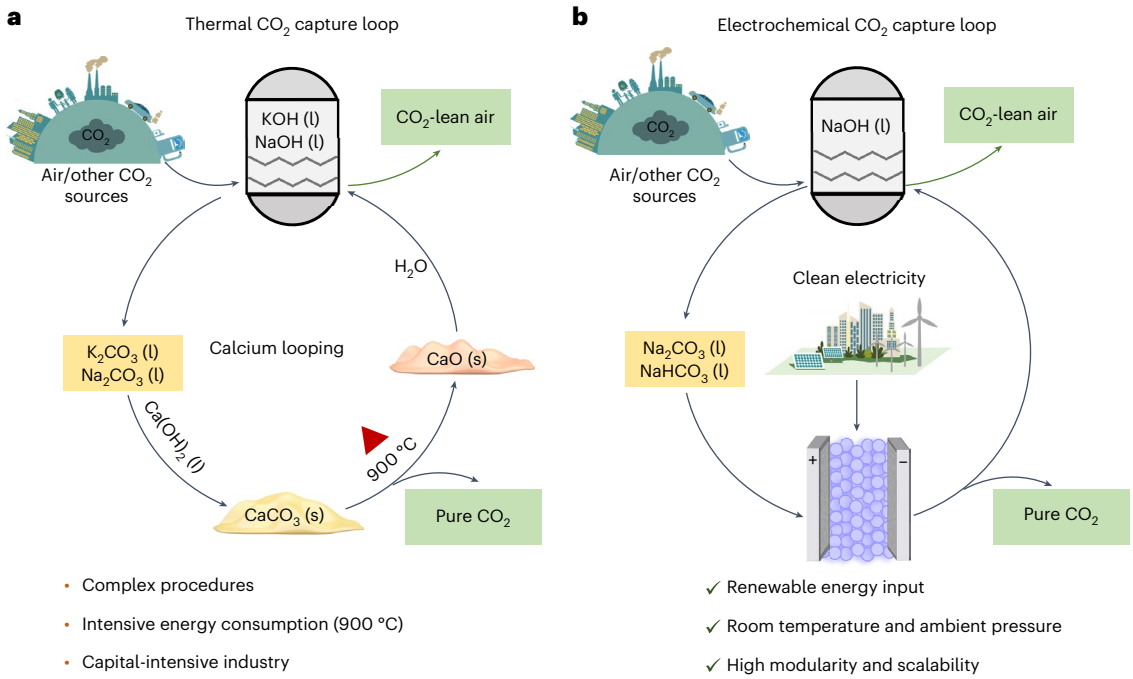

Fig. 1 | Comparison between thermal and electrochemical CO_2 regeneration in the CO_2–carbonate carbon capture loop. a, Schematic illustration of the pilot-scale CO_2 capture process via calcium carbonate looping. The CO_2 regeneration step involves high-temperature (900 °C) annealing of calcium carbonate, which consumes natural gas and a large portion of overall energy consumption. **b**, Schematic illustration of the electrochemical CO_2 regeneration from carbonate or bicarbonate solutions in our solid electrolyte reactor for a complete carbon capture loop.

carbonate compounds, its thermal regeneration process typically takes much higher energy than amine-based sorbents (Fig. 1a). For example, as demonstrated in a pilot scale[3], even converting more stable K_2CO_3 to $CaCO_3$ for calcination and hydroxide regeneration, it requires more than 900 °C heating, which contributes to a big portion of the overall energy consumption. More challenging, the heating source for thermal regeneration typically comes from the burning of fossil fuels (such as natural gas), which not only requires centralized infrastructure but also produces a large carbon footprint that has to be recaptured[3,5,6,16–18].

Electrochemical regeneration, which can use renewable electricity as the energy input, is considered as a green, efficient and sustainable alternative to the thermal regeneration counterpart to release CO_2 from the carbon-containing solutions[7–12,19–28]. The electrochemical reactions are operated under room temperature and ambient pressure, which avoids complicated infrastructure as in the case of thermal regeneration and are also energy efficient[19,22,25,29] (Fig. 1b). The working mechanism is typically based on the pH sensitivity of the carbon-containing solutions, such as the acidification of (bi)carbonate to regenerate high concentration of CO_2 via electrolysis-induced acid and alkaline solutions[30]. Representative examples including electrochemical pH swing or electrodialysis were demonstrated using cation exchange membrane (CEM), anion exchange membrane, bipolar membrane and their mixture modules[7,8,16,17,23]. However, these demonstrations are typically limited by complicated acid/alkaline separation and re-mixture steps[31,32], small CO_2 regeneration rates (or small operation current densities)[10,26] or generation of side products such as H_2, O_2 or Cl_2[33–36]. For instance, in a previous report of a conventional three-chamber electrolyser for carbonate regeneration, a cell voltage of over 2 V was needed to deliver a small current of 15 mA cm^{-2}, suggesting high energy consumption and low CO_2 regeneration rates that limit its practical applications[10]. Additionally, similar electrochemical devices were proposed to extract CO_2 from seawater for direct air capture applications[23,37–39], which however would suffer from the harsh seawater environments such as Ca^{2+}/Mg^{2+} impurities to clog membranes/electrodes, bacteria fouling, side reactions due to the high concentration of NaCl and so on. More importantly, the carbon capture rates and efficiencies reported in most of the seawater studies were based on pH measurements and equilibrium assumptions instead of direct CO_2 gas collections[8,23,26,31,37–40], which may not accurately reflect the carbon capture rates or energy consumptions when deployed in practice.

Here we reported an efficient electrochemical regeneration of high-purity CO_2 from aqueous (bi)carbonate in a modular solid electrolyte reactor for practical carbon capture applications. By performing hydrogen evolution reaction and hydrogen oxidation reaction (HER/HOR) redox electrolysis (or water splitting if H_2 product is desired), (bi)carbonate solutions can be continuously converted back into high-purity CO_2 gas at practical rates, during which high concentration of alkaline solutions is regenerated. Our reactor demonstrated high ion transport number, industrially relevant carbon capture rates, low energy consumptions, high capture capacity retention and good stability, suggesting a promising drop-in replacement of the conventional thermal regeneration processes.

Reactor design principle for CO_2 regeneration

The fundamental working mechanism of electrochemical CO_2 regeneration from carbonate solutions (such as Na_2CO_3 or $NaHCO_3$) is straightforward: by performing electrochemical reactions involving proton consumption (equivalent to OH^- generation) and generation on the cathode and anode, sodium and carbonate ions can be separated into the cathode and anode chamber via ion exchange membranes, respectively, to form NaOH and H_2CO_3. The formed H_2CO_3 simultaneously decomposes into CO_2 gas, whereas the NaOH solution can be fed back to air contactors. In traditional two-chamber membrane electrode assembly (MEA) devices or three-chamber electrodialysis devices (Fig. 2a), carbonate and protons are typically combined in the anode chamber where regenerated CO_2 gas will be inevitably mixed with either O_2 (in the case of oxygen evolution reaction (OER)) or unreacted H_2 (in the case of HOR). Electrochemically splitting salts (such as Na_2SO_4 or NaCl)

https://doi.org/10.1038/s41560-024-01654-z

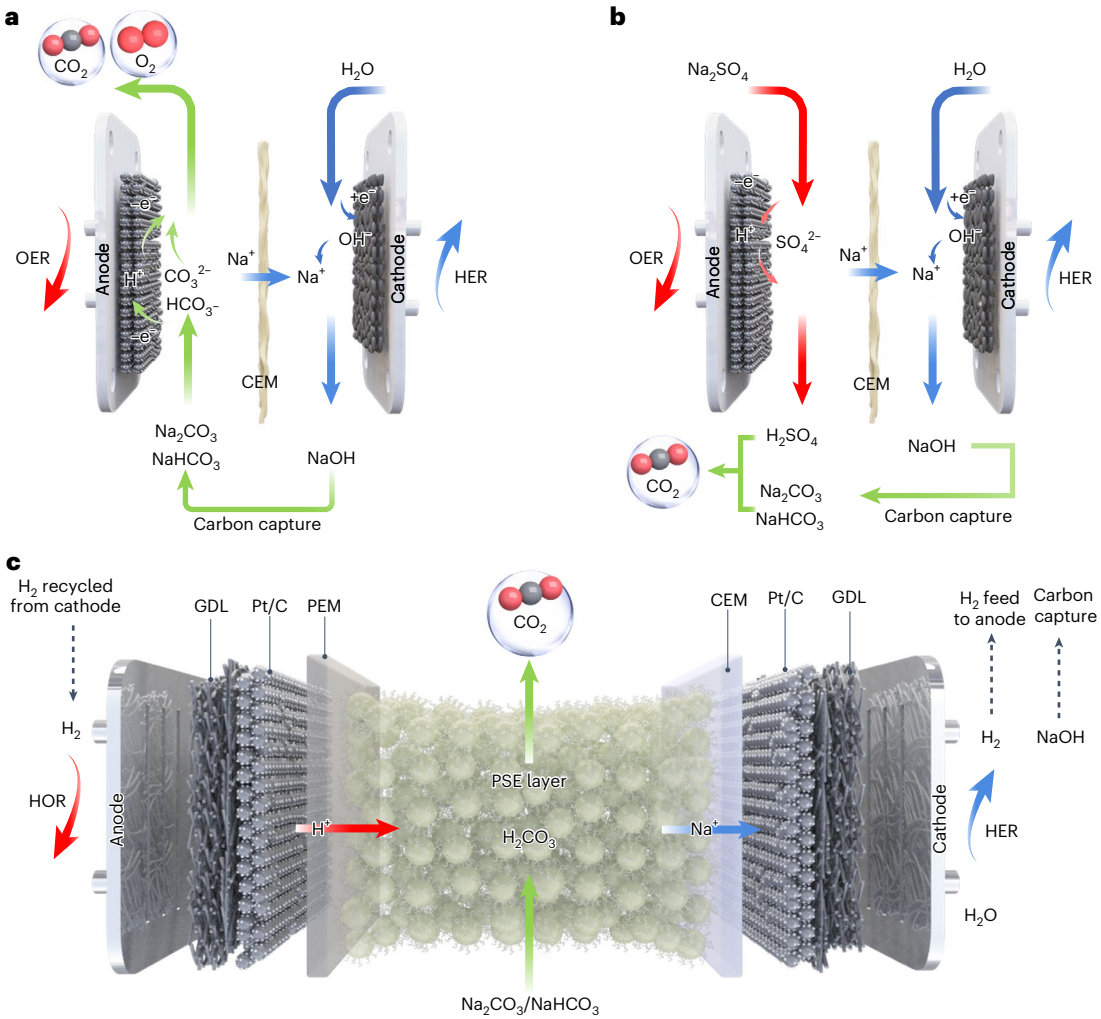

Fig. 2 | Comparison between our porous solid electrolyte reactor design and traditional electrolysers for CO_2 regeneration from (bi)carbonates. **a**, Schematic illustration of the traditional electrochemical CO_2 release process using a CEM-based MEA device. The regenerated CO_2 gas in the anode chamber is inevitably mixed with O_2 produced from the OER. **b**, Schematic illustration of the traditional pH swing method for carbon capture and release. Due to an acid/(bi)carbonate solution mixing step, this method typically involves excessive water to be evaporated to restore its original salt concentration, which consumes extra energy. In addition, the choices of half-cell reactions are restricted to gas evolution reactions due to liquid streams in both cathode and anode, resulting in excessive energy consumption to produce H_2 by-product. **c**, Our solid electrolyte reactor is designed for CO_2 regeneration from carbonate or bicarbonate solutions. It consists of a cathode for HER and an anode for HOR, a CEM and a PEM, and a layer of PSE layer sitting in between. This three-chamber solid electrolyte reactor design enables the regeneration of CO_2 in its high-purity form and does not involve excessive water to be evaporated nor any net products such as H_2 in the previous two cases.

into alkaline and acid, followed by carbon capture (via gas–alkaline contact) and CO_2 release (via carbonate–acid mixing), can effectively avoid this gas mixture issue (Fig. 2b). However, this salt splitting cycling process typically involves by-products such as H_2 or Cl_2 and excessive water to be evaporated to restore its original salt concentration, which consumes extra energy.

To address these challenges, here we report a three-chamber electrochemical reactor with a porous solid electrolyte (PSE) layer separated by a CEM and a proton exchange membrane (PEM) between cathode and anode for efficient and scalable CO_2 regeneration from carbonates (Fig. 2c and Supplementary Fig. 1). Please note that we used the terms PEM and CEM to differentiate their purpose of use: PEM was used when H^+ is the target ion and CEM was used when Na^+ or other alkali metal cations is the target ion (Methods). In this design, (bi) carbonate solutions will be continuously pumped into the PSE layer for regeneration, where the regenerated CO_2 gas will be separated from the cathode or anode gas during electrolysis. By continuously performing redox electrolysis, protons (H^+) generated at the anode/PEM interface will be electrically driven into the middle layer to replace the sodium ions (Na^+) that move across the CEM into the cathode chamber. As a result, Na_2CO_3/$NaHCO_3$ in the middle layer will be split into CO_2 in the middle chamber and NaOH solutions in the cathode chamber as regenerated absorbents. The PSE layer contains dense but water- and gas-permeable polymers (Supplementary Fig. 2) that are functionalized with cation-conducting sulfonate groups, which plays a central role in nucleating CO_2 bubbles and minimizing ohmic loss, especially under low salinity for low energy consumptions. We chose the HER/HOR redox couple due to their facile reaction kinetics when compared with other redox couples, such as oxygen reduction reaction and oxygen evolution reaction (ORR/OER) or water splitting. Please note here that typically HOR or ORR is not used in traditional two-chamber pH swing reactors where both the cathode and anode chambers have liquid streams that block gas transport channels. The key differences between this three-chamber reactor design and our group's recent carbon capture study[9] are also included in Supplementary Note 1, Supplementary Fig. 1, and Supplementary Tables 1 and 2.

https://doi.org/10.1038/s41560-024-01654-z

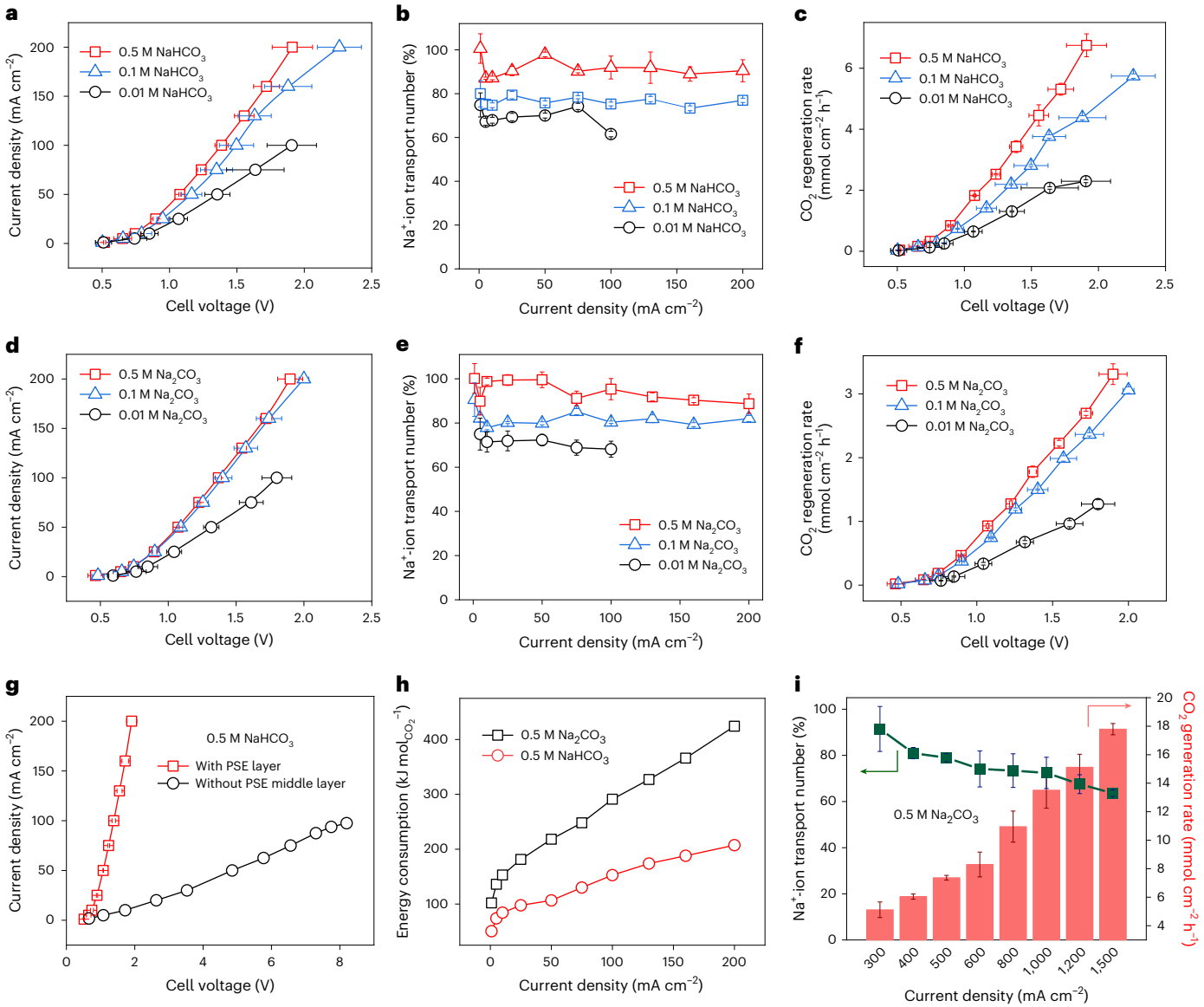

Fig. 3 | The CO_2 regeneration performance under a continuous flow of $NaHCO_3$ and Na_2CO_3 solutions through the middle PSE layer with different concentrations. a–**c**, The *I*–*V* curve (**a**), corresponding Na^+-ion transport number (**b**) and CO_2 regeneration rate (**c**) of our electrochemical device by directly flowing different concentrations of $NaHCO_3$ solution into the middle PSE layer. **d**–**f**, The *I*–*V* curve (**d**), corresponding Na^+-ion transport number (**e**) and CO_2 regeneration rate (**f**) of our electrochemical device with different concentrations of Na_2CO_3 solution into the middle PSE layer. **g**, The cell voltage comparison between the PSE and without PSE (sand filling with similar particle size) in the middle layer, where the PSE layer greatly decreases the cell resistance and voltage. When compared with the case of filling sands (with similar size to PSE particles) inside the middle layer compartment, under a 0.5 M $NaHCO_3$ solution flow, our PSE reactor saved a cell voltage of ~6.8 V when delivering a current density of 100 mA cm^{-2}, representing around 80% saving of energy consumption. **h**, The electrochemical energy consumption of CO_2 release (kJ mol$_{CO2}^{-1}$) as a function of the CO_2 regeneration rate under the flow of 0.5 M Na_2CO_3 or 0.5 M $NaHCO_3$ through the PSE layer. The onset energy consumption is as low as 50 kJ mol$_{CO2}^{-1}$ in 0.5 M $NaHCO_3$ solution, suggesting a high energy efficiency. **i**, The Na^+-ion transport number and corresponding CO_2 regeneration rates under higher current densities. The t_{Na+} can be maintained as high as over 60% when delivering industrially relevant current density of up to 1.5 A cm^{-2}. The error bars in **a**–**g** and **i** correspond to the standard deviation of three independent measurements. Data are presented as mean values ± s.d.

Electrochemical characterizations of the PSE reactor

Here we first introduce a few key parameters of the system including ion transport number (t_{Na^+}) of Na^+, CO_2 absorbent's capacity retention (CR) and energy consumption (Supplementary Note 2). Other important factors/parameters including the regenerated NaOH concentrations, CO_2 gas collection efficiency and operation stability will also be discussed in the study. Intrinsic electrochemical performances of our solid electrolyte reactor were first characterized under standard cell operation conditions (Fig. 3). Commercial Pt/C catalyst was used for both cathode HER and anode. The electrode active area was fixed at 1 cm^2 in this work unless otherwise noted. We first operated our cell by continuously flowing $NaHCO_3$ solutions through the PSE layer, with sufficient water flow at the cathode side to rapidly remove crossing-over interfacial Na^+ and minimize mass transport impacts. The onset potential of our device starts at ~0.5 V (under 1 mA cm^{-2}). Please note here that the cell voltages reported in this study were not iR compensated. The t_{Na^+} were kept high (>90%) across a wide range of current densities and cell voltages when 0.5 M $NaHCO_3$ was fed (Fig. 3b). This performance surpasses traditional bipolar membrane cell configurations,

https://doi.org/10.1038/s41560-024-01654-z

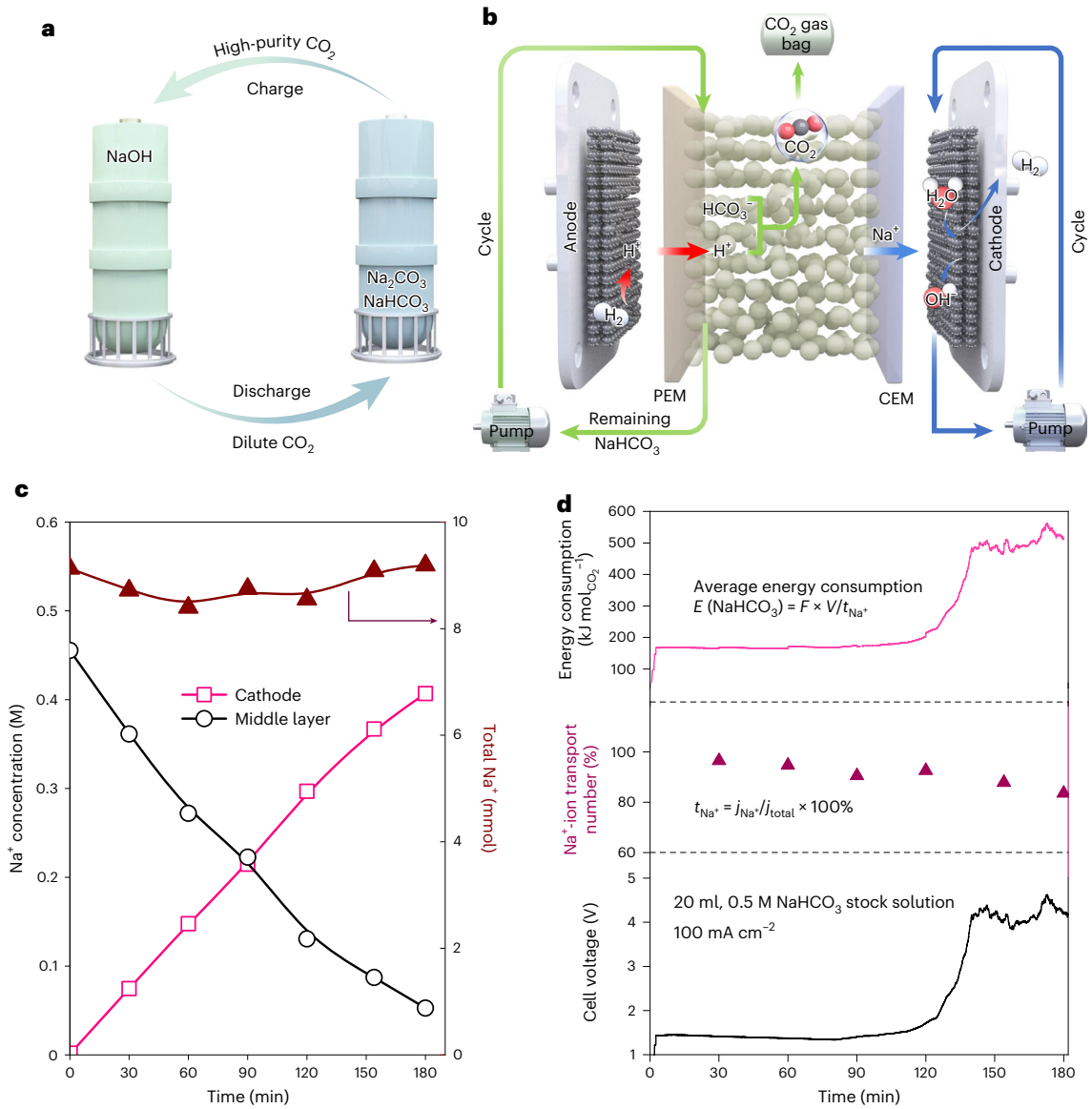

Fig. 4 | Carbon balance analysis in a electrolyte recirculation mode. a, The schematic illustration of a CO_2 capture and regeneration process is analogous to a battery's charging and discharging process. Assuming we start with a certain volume and concentration of NaOH solution, it represents the status of a fully charged battery. Once it reacts and absorbs CO_2 molecules from dilute sources, it is converted to Na_2CO_3 or $NaHCO_3$ depending on how deeply we discharge the 'battery'. The following CO_2 regeneration step represents the battery charging process where sodium carbonate or bicarbonate is converted back to NaOH while high-purity CO_2 is obtained, which closed the whole carbon capture loop. **b**, Schematic illustration of recirculation operation mode for CO_2 and NaOH regeneration. In an ideal case, if we can move all the Na^+ ions from the PSE layer into the cathode chamber, we can, in principle (assuming negligible volume changes in electrolyte), obtain the NaOH solution with the same concentration of input $NaHCO_3$ solution, collect 100% of CO_2 that has been captured and thus complete the whole carbon capture loop. **c**, The Na^+ concentration in the middle and cathode chamber as a function of electrolysis time. The total Na^+ mass remains almost unchanged during the electrocatalysis. **d**, The cell voltage, t_{Na^+} and energy consumption of our PSE reactor under recirculation operation mode. In these equations, E represents the energy consumption, F is the Faraday constant, V is the cell voltage, j_{Na^+} is the partial current density conducted by Na^+ ions and j_{total} is the total current density. The cell current density was maintained at 100 mA cm^{-2} and the electrode area was 1 cm^2.

particularly under industrial-relevant current densities[8,26] (Supplementary Table 3). The t_{Na^+} only slightly dropped to ~80% and 70% when the $NaHCO_3$ concentration dropped to 0.1 M and 0.01 M, respectively, suggesting our reactor's capability of pulling out most of Na^+ from the (bi)carbonate solution for a high capture capacity retention while maintaining high t_{Na^+}.

In principle, for every Na^+ transported into the cathode chamber, the corresponding bicarbonate anion will be balanced with one proton from the anode chamber to form one H_2CO_3 or CO_2. Therefore, the CO_2 regeneration rate can be calculated based on the operation current and the Na^+ ion transport number. In our practical demonstrations in the following section, we also obtained the CO_2 regeneration rates by CO_2 gas collection, which were close to the rate estimation based on measured electrochemical performances. As shown in Fig. 3c, under the 0.5 M $NaHCO_3$ input, a CO_2 regeneration rate of 6.78 mmol cm^{-2} h^{-1} CO_2 gas was achieved while maintaining a 90% t_{Na^+} under a practical operation current density of 200 mA cm^{-2}. Whereas the regeneration rate decreased with lower Na^+ concentration, it can still reach >2 mmol cm^{-2} h^{-1} even under 0.01 M solution.

Whereas converting NaOH to bicarbonate in air contactors would double the carbon capture capacity and energy efficiency compared with that of carbonate, the practical CO_2 absorption process may stop

at the carbonate stage due to the low CO_2 concentrations in air. Unlike $NaHCO_3$ solution where CO_2 gas can be readily released under a net H^+ flux into the middle layer, the Na_2CO_3 solution needs to be acidified into $NaHCO_3$ first before CO_2 gas bubbles can be regenerated, which doubles the energy consumption. As shown in Fig. 3d–f, the current–voltage (*I*–*V*) curves and corresponding Na^+-ion transport number using 0.5 M, 0.1 M and 0.01 M Na_2CO_3 are similar to that of $NaHCO_3$, except for the CO_2 regeneration rates that are roughly half of that in the case of $NaHCO_3$.

The indispensable role of the PSE layer can be shown in Fig. 3g, Supplementary Figs. 3 and 4, and Supplementary Table 3. This improved cell voltage was due to the significantly decreased cell impedance with the help of ion conductions through the sulfonate functional groups along the surface of PSE particles[41,42]. This improved ion conduction and decreased cell voltage guarantee an energy efficient CO_2 regeneration process as shown in Fig. 3h. The energy consumption starts from 50 kJ mol_{CO2}^{-1} in the case of $NaHCO_3$ and gradually increases with ramped-up regeneration rates. The low energy consumption enables our design to be more energy efficient than conventional high-temperature annealing of calcium carbonate process (Supplementary Fig. 5) and some other electrochemical systems (Supplementary Fig. 6).

To show the upper limit of our device's CO_2 regeneration rate, we increased the Na_2CO_3 solution flow rate to 9 ml min^{-1} and achieved industrially relevant current densities of up to 1.5 A cm^{-2} while maintaining a high t_{Na^+} of 65%, representing a CO_2 generation rate of ~18 mmol cm^{-2} h^{-1}. However, this continuous electrolyte flow typically results in low capacity retention because only a fraction of Na^+ was pulled out from the middle layer for NaOH regeneration (Supplementary Note 3 and Supplementary Fig. 7). As more practical demonstrations shown below, we operated the regeneration process in batch cycles to balance both the t_{Na^+} and capture capacity retention.

The PSE reactor design also showed good adaptability to be operated under different cathode or anode reactions. When switching HOR on the anode side to water oxidation (OER), net H_2 generation can be obtained from the cathode with an extra cell voltage input (Supplementary Fig. 8). The onset cell voltage of this HER/OER cell was at ~2 V and is ~1.5 V higher than that of HER/HOR, suggesting an extra energy consumption of 40.2 kWh kg_{H2}^{-1} for clean H_2 manufacturing. This HER/OER cell configuration opens opportunities in combining water electrolysis with carbon capture in a single electrolyser device, which could lower both capital and operation cost in carbon capture and clean H_2 production. Changing half-cell reactions does not affect the Na^+-ion transport number, which were well maintained at above 80% across a wide range of cell currents (Supplementary Fig. 8b). We also found out that different types of CEM used could affect the t_{Na^+}. As an alternative to the Nafion N2100TX membrane, we have identified a PTFE fabric-reinforced Nafion membrane, which has shown similar performance to the original Nafion N2100TX membrane (Supplementary Fig. 9). However, the use of Nafion-117, a well-known proton conductor, on the cathode side improves H^+ conduction and thus decreases our t_{Na^+} (Supplementary Fig. 10).

Na^+ balance analysis under electrolyte recirculation mode

Our next step is to explore its CO_2 regeneration capability under more practical operation conditions. In practice, the CO_2 capture and regeneration process are analogous to a battery's discharging and charging process, respectively (Fig. 4a). To fulfil these charging/discharging cycles, we operated our PSE device for CO_2 regeneration, or the charging step, under an electrolyte recirculation mode (Fig. 4b) and performed a Na^+ mass balance analysis (Fig. 4c). Specifically, we recirculated 20 ml $NaHCO_3$ solution in the middle PSE layer and 20 ml deionized (DI) water in the cathode chamber, respectively, during the CO_2 regeneration electrolysis. A detailed Na^+ mass balance analysis can help us to not only obtain critical parameters including t_{Na^+} and CR but also confirm the high accuracy of our measurements under this practical operation mode.

The Na^+ concentrations at both the cathode and middle layer and the cell voltage were monitored during the electrolysis process under a fixed current of 100 mA cm^{-2} (Fig. 4c,d). Whereas the concentration of the as-prepared $NaHCO_3$ solution was 0.5 M, the measured concentration at the starting point of electrolysis was ~0.45 M, which could be due to a small amount of Na^+/H^+ ion exchange in the PSE layer. Under continuous HER/HOR electrolysis, the Na^+ concentration in the middle layer gradually decreased and that in the cathode increased, with the total Na^+ mass well-balanced across the whole electrolysis process (Fig. 4c). After a 3-hour continuous electrolysis, the middle layer Na^+ concentration was down to ~0.05 M, which represents a 90% removal of Na^+ or 90% capture capacity retention. If in practice the initial $NaHCO_3$ concentration starts from 1 M, the capacity retention can reach 95% when the middle layer is depleted to 0.05 M. More importantly, achieving this high capacity retention did not sacrifice t_{Na^+}. As shown in Fig. 4d, the t_{Na^+} was maintained at above 80% across the whole 'charging' process. Another interesting observation we had was the cell voltage shown in Fig. 4d. Whereas it was maintained stable at ~1.4 to 1.5 V for the first 2-hour operation, the cell voltage rapidly increased to ~4 V when the 'charging' process approached the end (Supplementary Note 4 and Supplementary Fig. 11). This rapid increase in the cell voltage can serve as an indicator of middle layer Na^+ depletion, where a cut-off cell voltage can be flexibly set to stop the regeneration step and complete the carbon capture loop while maintaining a good t_{Na^+} and energy efficiency (to be shown in Fig. 5).

Stability test and CO_2 gas collection

To evaluate the stability and actual CO_2 gas collection, we increased the volume of recirculation liquid to 400 ml and the electrode size to 4 cm^2 while maintaining a fixed electrolysis current density of 100 mA cm^{-2} (400 mA total cell current). The electrolysis operation was cut off at ~4.5 V as the end of the 'charging' step for each carbon

Fig. 5 | Practical cycle operations for CO_2 regeneration in our PSE reactor. **a**, The chronopotentiometry stability of the PSE reactor for cycles of CO_2 regeneration. The volume of $NaHCO_3$ stock solution and catholyte in the first cycle were both 200 ml and then changed to 400 ml for the following cycles. The concentration of the $NaHCO_3$ stock solution was 0.5 M, and the total cell current was 400 mA with an electrode area of 4 cm^2 (current density is 100 mA cm^{-2}). In these equations, n is the number of electrons involved, F is the Faradaic constant, j_{total} is the total current density, and M_0 and M_1 represent the Na^+ mass before and after the cycling process. Alternating yellow and white backgrounds represent different batch tests. The PSE reactor can stably run for more than 100 h. In principle, for every mole of Na^+ transported from PSE layer to the cathode chamber, we should be able to collect a mole of CO_2 from the PSE layer due to the complete acidification of a mole of HCO_3^-, meaning that the t_{Na^+} measured by the catholyte Na^+ concentration should be equal to the FE_{CO_2} when we assume $1e^-$ transfer per CO_2 molecule collected in the case of $NaHCO_3$ solution. **b**, Photograph of the solid electrolyte reactor and as-captured CO_2 gas flowing out from PSE layer. **c**, The *I*–*V* curve and corresponding t_{Na^+} when inputting the carbon-containing solution obtained from direct air capture. **d**, Approaches to further improving the energy consumption: cell voltages (at 50 mA cm^{-2} and 200 mA cm^{-2}) of PSE reactors with different CEM thicknesses (50 µm versus 200 µm), different PSE layer thicknesses (2.0 mm versus 2.5 mm) and different operation temperatures (room temperature (r.t.), 60 °C and 90 °C). **e**, Roadmap to CO_2 regeneration cost by successive changes to cost-relevant parameters. **f**, Sensitivity analysis of the CO_2 regeneration cost based on $NaHCO_3$ and Na_2CO_3 inputs, with variables including electricity price, current density, cell voltage, stack cost and Na^+-ion transport number.

https://doi.org/10.1038/s41560-024-01654-z

capture and regeneration cycle (Fig. 5a and Supplementary Fig. 12). Benefiting from the reliable Pt/C catalyst and commercial CEM and PEM membranes, our PSE reactor exhibited excellent long-term stability and CO_2 gas regeneration efficiency from bicarbonate solution. The cell voltage was maintained stable at ~1.7 to 1.9 V and quickly ramped up to over 4 V at the end of each cycle (~12 h of continuous electrolysis for 400 ml stock solution). We can evaluate the cell's electron efficiency in carbon regeneration based on either the t_{Na^+} or more directly on the collected CO_2 gas volume (Fig. 5a). We therefore also defined the Faradaic efficiency (FE) of collected CO_2, in the case of bicarbonate input,

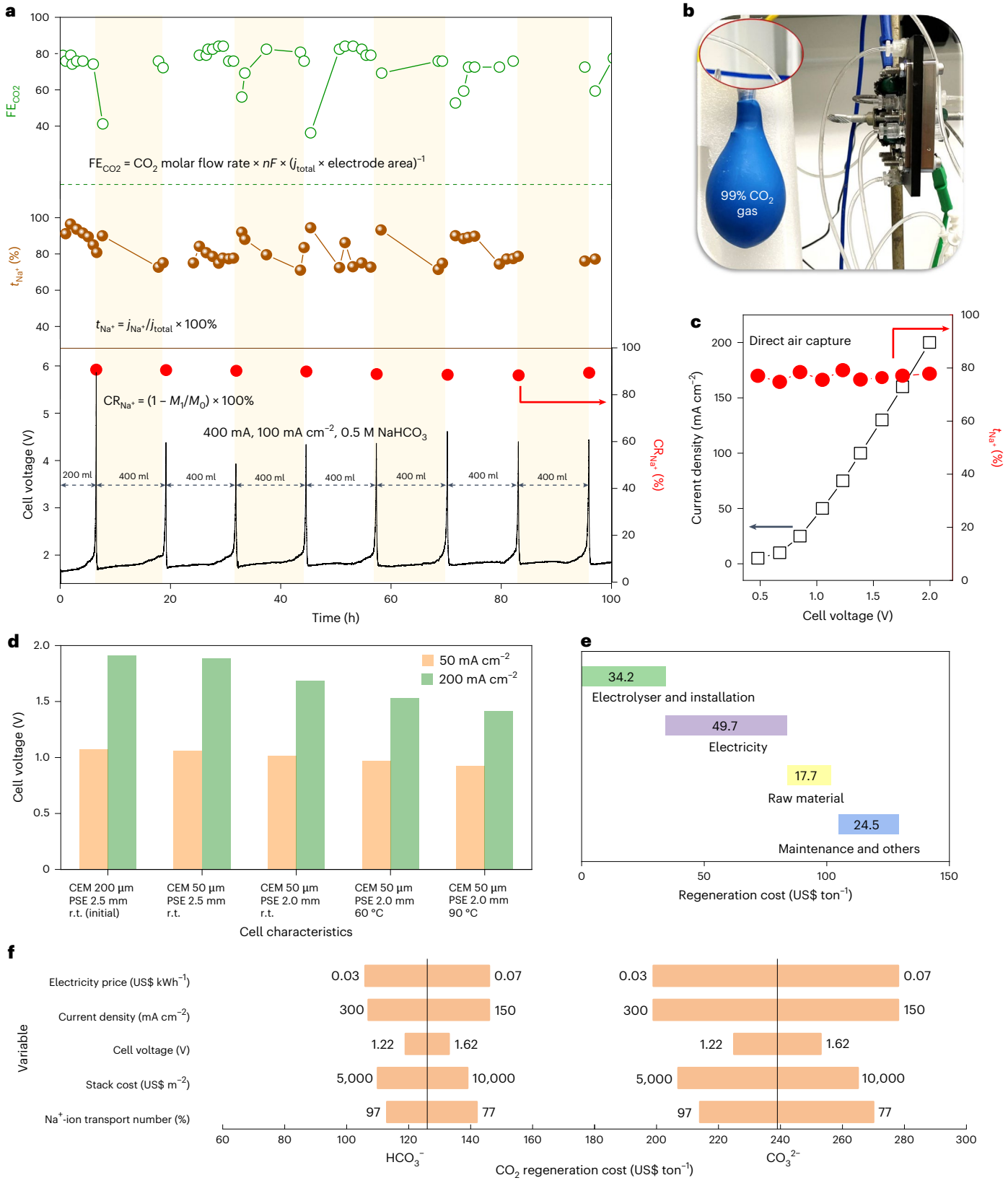

as the total number of CO_2 molecules regenerated over the total number of electrons transferred. This test can distinguish our study from many previous ones where no CO_2 gas collections were performed, and the energy consumptions were estimated solely based on pH equilibriums[24,32,35]. In each electrolysis cycle, the t_{Na^+} started at ~90% when there was sufficient Na^+ in the middle PSE layer and gradually decreased to 70 to 80% at the end of the cycle (assuming negligible volume change in both cathode and PSE layer electrolytes), which is due to the gradually increased Na^+ concentration gradient across the CEM. In fact, we observed an approximately 5–8% volume increase in the catholyte at the end of each cycle due to osmosis effects. This slight volume increase suggests that our calculated t_{Na^+} was slightly underestimated. At the end of each cycle, around 90% carbon capture capacity retention was achieved.

The collection and measurement of regenerated CO_2 gas from our PSE reactor are of central importance to support the analysis of carbon regeneration energy consumptions based on cell voltage and Na^+-ion transport number. As a visual demonstration, an empty balloon (~100 ml size) was filled with recovered CO_2 gas from the PSE layer (Fig. 5b). We first used gas chromatography to confirm the purity of CO_2 gas collected (>99%; Supplementary Fig. 13 and Supplementary Table 4). As shown in Fig. 5a, by measuring the regenerated CO_2 gas flow rate using the water displacement method (Methods), we were able to quantify the FE_{CO_2} of our reactor. We observed that, due to an initial CO_2 saturation process in the 400 ml $NaHCO_3$ electrolyte, the CO_2 output flow rate usually started lower at the beginning of each regeneration cycle but rapidly reached to a steady state of around 4.5–5.1 ml min^{-1}, representing a 75%~85% FE_{CO_2} (Fig. 5a). Whereas the measured FE_{CO_2} was slightly lower than the corresponding t_{Na^+}, which is highly likely due to gas leakage in the reactor system (Supplementary Fig. 14), the two values are close enough to strongly support our hypothesized CO_2 regeneration mechanism and Na^+ quantifications. The cell can be operated for more than 100 h with negligible degradation. To confirm the remaining carbon sources in the reactor system, the residual $NaHCO_3$ solution and catholyte NaOH solution after each regeneration cycle were further analysed using the acid titration method[43] (Supplementary Fig. 15 and Supplementary Note 5). In practice, this remaining $NaHCO_3$ solution can be reused as the catholyte in the next round of carbon regeneration. No carbon was found in the catholyte, indicating no CO_2 or bicarbonate crossover contamination in the regenerated NaOH solution. As proof-of-concept, we also demonstrated a full-loop direct air capture process by bubbling air into NaOH solution to form Na_2CO_3/$NaHCO_3$ solution, which was fed into our PSE reactor for CO_2 and NaOH regeneration. No obvious electrochemical performance deviations were observed when compared with the standard tests (Fig. 5c, Supplementary Note 6 and Supplementary Figs. 16–18).

Performance improvements and techno-economic analysis

Whereas our PSE reactor design for carbon regeneration showed great promise in energy consumption, we would like to emphasize that these electrochemical performances are not fully optimized yet. There are many optimizations can be done in the future to further improve the efficiency of our reactor, such as improving the ionic conductivity of the solid electrolyte particles, shrinking the thickness of the PSE layer, increasing the operation temperature, improving the HER and HOR catalysts, selecting more conductive CEMs and PEMs and so on. Here we performed additional experiments to demonstrate some representative factors that can help to significantly improve the energy efficiency particularly under high operation current densities (Fig. 5d, Supplementary Note 7, Supplementary Figs. 6 and 19, and Supplementary Table 3). Whereas these improvements in energy consumption are encouraging, future efforts are needed to further optimize the reactor and process for practical applications.

On the basis of the electrochemical performance of our PSE reactor system for CO_2 regeneration, we performed a techno-economic analysis (TEA) to assess its economic viability and adaptability, adapting previously reported methods[17,44,45]. Several process assumptions were made based on current feedstock prices and electrolyser performance, with sensitivity analysis considering potential fluctuations in these values in the future. The analysis of $NaHCO_3$ input case indicates a total system cost of approximately US$126 ton_{CO2}^{-1} (Fig. 5e,f and Supplementary Note 8). The primary cost is contributed by electrolyser stack manufacturing (US$34.2 ton_{CO2}^{-1}), raw material (US$17.7 ton_{CO2}^{-1}) and electricity (US$49.7 ton_{CO2}^{-1} assuming US$0.05 kWh^{-1} electricity price). Other expenses, including daily maintenance and stack replacement, account for approximately 19.4% of the total cost. Further improvements can be achieved by reducing the cost of the electrolyser and enhancing the reaction performance. By reducing the cell voltage and increasing the Na^+-ion transport efficiency, we can further reduce the carbon capture cost of our device by ~US$7 and ~US$13 ton_{CO2}^{-1}, respectively (Fig. 5f). A more detailed global sensitivity analysis (Supplementary Figs. 20–22) reveals that the regeneration cost is highly sensitive to variations in electricity price (ranging from US$0.03 to US$0.07 kWh^{-1}) and current density (ranging from 150 mA cm^{-2} to 300 mA cm^{-2}). This is because, based on the TEA calculations in Supplementary Note 8, electricity price is associated with operating costs, whereas current density relates to the electrolyser size and capital cost for a fixed duty of 1 ton CO_2 capture. These two parameters dominate the operation cost and capital cost. Other parameters, such as cell voltage, have a relatively moderate impact on the regeneration cost. Therefore, it is essential to develop strategies to mitigate associated risks, such as avoiding current density drops under certain voltage changes. Additionally, monitoring policy changes and fluctuations in the electricity grid and price will help maintain an economically feasible CO_2 capture and regeneration process. The carbon regeneration cost of carbonate input is nearly double that of bicarbonate, due to doubled size of electrolysers and doubled energy consumption, whereas the sensitivity analysis shows a similar tendency. Nonetheless, the development of renewable energy technologies and improvements in electrolysers can be leveraged to decrease the regeneration cost in the near future.

Conclusions

In conclusion, we developed an electrochemical system to efficiently regenerate high-purity CO_2 gas and alkaline absorbents from (bi) carbonate solutions. By performing HER and HOR redox electrocatalysis, our PSE device can efficiently extract CO_2 molecules from carbon-containing solution to high-purity (99%) CO_2 stream without mixing other gases. Industrially relevant carbon capture rates (up to 964.5 mA cm^{-2}, 18 mmol cm^{-2} h^{-1} or 190 kg_{CO2} m^{-2} d^{-1}) were achieved. Moreover, high Na^+-ion transport number (>90%), high capacity retention (~90%) and low energy consumptions (50 and 118 kJ mol_{CO2}^{-1} at 1 and 100 mA cm^{-2} for bicarbonate, respectively) were demonstrated, suggesting its promising practical applications. With improvements in cell components and operation temperature, a cell voltage of 1.42 V at a current density of 200 mA cm^{-2} was achieved. Future research will be focused on the scaling up of this PSE reactor for large-scale CO_2 regeneration from carbonate solutions and further improvements in cell design and configurations for better voltages, current densities and energy efficiencies.

Methods

Materials

All chemicals, including sodium hydroxide (NaOH), sodium carbonate (Na_2CO_3), sodium bicarbonate ($NaHCO_3$) and Nafion-117 solution, were purchased from Sigma-Aldrich. Pt/C powder, Nafion-117 membrane and Nafion-N2100TX membrane were purchased from Fuel Cell Store. IrO_2 electrode was purchased from the Dioxide Materials. Millipore water (18.2 MΩ·cm) was used throughout all experiments.

Preparation of Pt/C electrodes for HER reaction

Typically, 40 mg active catalyst (Pt/C) and 80 µl of Nafion-117 binder solution were mixed with 4 ml of 2-propanol (Sigma-Aldrich). After sonication in ice water for 30 min, the obtained homogeneous ink was air-brushed onto a 5 × 5-cm^2 hydrophilic carbon cloth (ELAT-Hydrophilic Plain Cloth, Fuel Cell Store) electrode at 60 °C. Then the as-prepared electrode was hot-pressed on the Nafion-N2100TX membrane at 90 °C for 10 min.

Preparation of Pt/C electrodes for HOR reaction

The procedure of fabrication Pt/C anodes for HOR reaction followed the same procedure to prepare the cathode electrode, except the hydrophobic gas diffusion layer (GDL) carbon paper (Sigracet 28 BC, Fuel Cell Store) was used. Briefly, after sonication of the mixture of 40 mg active catalyst (Pt/C), 80 µl of Nafion-117 binder and 4 ml of 2-propanol, the obtained homogeneous ink was air-brushed onto a 5 × 5-cm^2 GDL (Sigracet 28 BC, Fuel Cell Store) electrode at 60 °C. Then the prepared electrode was further dried in a vacuum at room temperature before use.

PSE reactor with CEM–PEM configuration

The CO_2 recovery process was conducted in a solid electrolyte cell. The cell configurations and the production set-up are illustrated in Fig. 2c. The cation exchange membrane (CEM) close to the cathode (Pt/C on carbon cloth) is Nafion N2100TX (or PTFE fabric-reinforced Nafion alternatives), and the proton exchange membrane (PEM) close to the anode side (Pt/C on carbon paper) is the Nafion-117 membrane. The cathode side was supplied with DI water for HER reaction. The water flow rate was controlled by a syringe pump. The flow rate at the outlet was calibrated using a measuring cylinder. In the middle chamber, the sodium form styrene-divinylbenzene sulfonated copolymer Dowex 50WX8 (Sigma-Aldrich) cation conductor was employed as the solid electrolyte (SE). The Na_2CO_3 or $NaHCO_3$ flowed into the SE layer controlled by a syringe pump. The anode side was provided with the 30 sccm H_2 gas for HOR reaction. All cell resistance was measured by the potentiostatic electrochemical impedance spectroscopy (PEIS), and all the cell voltages in our work were reported without any IR compensation.

Batch cycles of CO_2/absorbent regeneration with recirculation of carbon-containing solution and catholyte

To maximally release CO_2 from the $NaHCO_3$/Na_2CO_3 solution, the H^+ produced at the anode should ideally react with all HCO_3^-/CO_3^{2-} groups. Therefore, a closed-loop recirculation system was developed. The cell configuration and experiment set-up are schematically shown in Fig. 4b. In batch cycles stability test (Fig. 5), a certain volume of 0.5 M $NaHCO_3$ solution (200 ml for the first cycle and 400 ml for other cycles) was supplied into the middle SE layer with a flow rate of 4.5 ml min^{-1} controlled by a syringe pump. At the anode side, the H_2 gas was supplied with a flow rate of 30 sccm. At the cathode, the same volume of DI water (200 ml for the first cycle and 400 ml for other cycles) was cycled with a flow rate of 4.5 ml min^{-1}. Along with the reaction proceeding, the carbon-containing solution in the middle SE layer would be gradually acidified to release CO_2 gas. Once the concentration of Na^+ in the middle chamber decreases to a low concentration, the cell voltage will be increased suddenly. To start a new batch, fresh 0.5 M $NaHCO_3$ and DI water were first flowed into the middle chamber and cathode respectively for 10 min to remove residue Na^+, and then fresh 0.5 M $NaHCO_3$ (400 ml) and DI water (400 ml) were used respectively. The residual Na^+ from the middle SE layer and the concentration of NaOH produced at the cathode were determined by using inductively coupled plasma optical emission spectroscopy (ICP-OES; Perkin Elmer Optima 8300 ICP-OES) and ion chromatography (IC; Shimadzu Prominence Ion Chromatography System for Cation Analysis).

Direct air capture

The direct air capture was operated in a plastic flask. The air was purged into 1.0 N NaOH solution through a gas dispersal tube. The gas bubbles were dispersed into small bubbles to increase the capture efficiency of CO_2. The Na^+ concentration of the final product was determined using ICP and IC, and the residual CO_3^{2-} and HCO_3^- were determined by using the titration method.

Middle layer gas and liquid analysis

After recycling electrolysis, the dissolved CO_2 and remaining carbon content (in the form of HCO_3^-) in the liquid was measured using the acid titration method. First, 4 ml of the middle layer output stream containing dissolved CO_2 was collected directly with adding 200 µl of 1 M NaOH. And then the collected liquid was titrated using 0.1 M HCl. The titrant was dropped slowly into the sample and the change of pH was monitored using a pH meter (Orion Star A111). The volume difference between two equivalence points on the titration curve determines how many moles of (bi)carbonate species exist inside the liquid samples. The dissolved CO_2 and remaining carbon concentration was then calculated as below:

$$Q_1 = \frac{\Delta V_1 \times c}{V}$$

For only detection of the remaining carbon content (in the form of HCO_3^-), 4 ml of the middle layer output stream containing dissolved CO_2 was collected without adding NaOH. And continuous Ar flow was used to purge out the dissolved CO_2 after the sample collection. Then we followed the same titration procedure as mentioned above. And the remaining carbon concentration was then calculated as below:

$$Q_2 = \frac{\Delta V_2 \times c}{V}$$

where Q_1 is the total remaining carbon concentration, Q_2 is the total remaining carbon concentration (in the form of HCO_3^-) and $(Q_1 - Q_2)$ is the dissolved CO_2 concentration. ΔV_1 and ΔV_2 are the volumes of HCl between two equivalence points on the titration curve, c is the concentration of the HCl solution used, and V is the volume of the sample titrated (without including the volume of the added NaOH).

Water displacement measurement was used to measure the gaseous CO_2 flow rate and released CO_2 volume. CO_2-saturated 0.01 M H_2SO_4 was used as the solvent during the water displacement measurement to measure the CO_2 bubble flow rate. It was pre-saturated with CO_2 to minimize the gas dissolution, and the acid was used to further suppress the CO_2 gas solubility during the bubble flow rate measuring process. This water displacement showed high measurement accuracy.

Ion transport number, Faradaic efficiency and CO_2 gas collection efficiency calculations

Na^+-ion transport number (t_{Na^+}) describes the ratio of the number of Na^+ ions crossed through CEM over the total number of electrons transferred during electrolysis.

The concentration of Na^+ was determined using ICP and IC. The transport number of Na^+ at the cathode under continuous catholyte flowing was calculated using the following equation:

$$j_{Na^+} = c \times \upsilon \times F \times (\text{electrode area})^{-1}$$

$$t_{Na^+} = \frac{j_{Na^+}}{j_{total}} \times 100\%$$

where c is the Na^+ concentration determined by ICP, υ is the catholyte flow rate (ml s^{-1}) and F is the Faradaic constant.

In the case of catholyte recirculation, the ion transport number for Na^+ is calculated using the following equation:

$$t_{Na^+} = \frac{c_{Na^+}\,(\mathrm{mol\,l^{-1}}) \times 96,485\,\left(\mathrm{C\,mol^{-1}}\right) \times \text{catholyte volume (ml)}}{j_{\text{total}}\,(\mathrm{mA}) \times \text{reaction time(s)}} \times 100\,(\text{maximum } 100\%)$$

FE_{CO_2} is defined as the ratio of the total number of CO_2 molecules regenerated over the total number of electrons transferred. It describes the electron efficiency in releasing CO_2 molecules.

Faradaic efficiency for CO_2 gas regeneration in the case of $NaHCO_3$ was calculated as below:

$$I_{CO_2} = \frac{v}{V_{\text{mol}}} \times nF$$

$$FE_{CO_2} = \frac{I_{CO_2}}{I_{\text{total}}} \times 100\%$$

where v is the gaseous CO_2 volumetric flow rate (ml s^{-1}) determined by the water displacement method, V_{mol} is the volume of an ideal gas at room temperature, n is the number of electrons involved ($n = 1$ for bicarbonate case and $n = 2$ for carbonate case) and F is the Faradaic constant.

Capacity retention of Na^+ (CR_{Na^+}) is defined as the following:

$$\text{Capacity retention} = \left(1 - \frac{M_1}{M_0}\right) \times 100\%$$

M_0 and M_1 represent the Na^+ mass in the middle PSE layer electrolyte before and after reaction, respectively, determined using ICP and IC.

Data availability

The data supporting the findings of this study are available in the main text, Supplementary Information and source data provided with this paper. Additional data related to this study may be requested from the corresponding author. Source data are provided with this paper.

References

1. Chu, S. Carbon capture and sequestration. *Science* **325**, 1599 (2009).
2. Goeppert, A., Czaun, M., Prakash, G. S. & Olah, G. A. Air as the renewable carbon source of the future: an overview of CO_2 capture from the atmosphere. *Energy Environ. Sci.* **5**, 7833–7853 (2012).
3. Keith, D. W., Holmes, G., Angelo, D. S. & Heidel, K. A process for capturing CO_2 from the atmosphere. *Joule* **2**, 1573–1594 (2018).
4. Buckingham, J., Reina, T. R. & Duyar, M. S. Recent advances in carbon dioxide capture for process intensification. *Carbon Capture Sci. Technol.* **2**, 100031 (2022).
5. Sanz-Pérez, E. S., Murdock, C. R., Didas, S. A. & Jones, C. W. Direct capture of CO_2 from ambient air. *Chem. Rev.* **116**, 11840–11876 (2016).
6. Rochelle, G. T. Amine scrubbing for CO_2 capture. *Science* **325**, 1652–1654 (2009).
7. Voskian, S. & Hatton, T. A. Faradaic electro-swing reactive adsorption for CO_2 capture. *Energy Environ. Sci.* **12**, 3530–3547 (2019).
8. Eisaman, M. D. et al. CO_2 extraction from seawater using bipolar membrane electrodialysis. *Energy Environ. Sci.* **5**, 7346–7352 (2012).
9. Zhu, P. et al. Continuous carbon capture in an electrochemical solid-electrolyte reactor. *Nature* **618**, 959–966 (2023).
10. Shu, Q., Legrand, L., Kuntke, P., Tedesco, M. & Hamelers, H. V. Electrochemical regeneration of spent alkaline absorbent from direct air capture. *Environ. Sci. Technol.* **54**, 8990–8998 (2020).
11. Liu, J. et al. Hydrogen-motivated electrolysis of sodium carbonate with extremely low cell voltage. *Chem. Commun.* **54**, 3582–3585 (2018).
12. Muroyama, A. P. & Gubler, L. Carbonate regeneration using a membrane electrochemical cell for efficient CO_2 capture. *ACS Sustain. Chem. Eng.* **10**, 16113–16117 (2022).
13. Bougie, F. & Fan, X. Microwave regeneration of monoethanolamine aqueous solutions used for CO_2 capture. *Int. J. Greenh. Gas. Control* **79**, 165–172 (2018).
14. Bougie, F. & Iliuta, M. C. Analysis of regeneration of sterically hindered alkanolamines aqueous solutions with and without activator. *Chem. Eng. Sci.* **65**, 4746–4750 (2010).
15. Yoo, M., Han, S.-J. & Wee, J.-H. Carbon dioxide capture capacity of sodium hydroxide aqueous solution. *J. Environ. Manag.* **114**, 512–519 (2013).
16. Halliday, C. & Hatton, T. A. Sorbents for the capture of CO_2 and other acid gases: a review. *Ind. Eng. Chem. Res.* **60**, 9313–9346 (2021).
17. Stolaroff, J. K., Keith, D. W. & Lowry, G. V. Carbon dioxide capture from atmospheric air using sodium hydroxide spray. *Environ. Sci. Technol.* **42**, 2728–2735 (2008).
18. Watkins, J. D. et al. Redox-mediated separation of carbon dioxide from flue gas. *Energy Fuels* **29**, 7508–7515 (2015).
19. Renfrew, S. E., Starr, D. E. & Strasser, P. Electrochemical approaches toward CO_2 capture and concentration. *ACS Catal.* **10**, 13058–13074 (2020).
20. Rheinhardt, J. H., Singh, P., Tarakeshwar, P. & Buttry, D. A. Electrochemical capture and release of carbon dioxide. *ACS Energy Lett.* **2**, 454–461 (2017).
21. Eisaman, M. D., Alvarado, L., Larner, D., Wang, P. & Littau, K. A. CO_2 desorption using high-pressure bipolar membrane electrodialysis. *Energy Environ. Sci.* **4**, 4031–4037 (2011).
22. Sharifian, R., Wagterveld, R., Digdaya, I., Xiang, C.-X. & Vermaas, D. Electrochemical carbon dioxide capture to close the carbon cycle. *Energy Environ. Sci.* **14**, 781–814 (2021).
23. Willauer, H. D., DiMascio, F., Hardy, D. R. & Williams, F. W. Development of an electrolytic cation exchange module for the simultaneous extraction of carbon dioxide and hydrogen gas from natural seawater. *Energy Fuels* **31**, 1723–1730 (2017).
24. Gurkan, B. et al. Perspective and challenges in electrochemical approaches for reactive CO_2 separations. *iScience* **24**, 103422 (2021).
25. Xia, R., Overa, S. & Jiao, F. Emerging electrochemical processes to decarbonize the chemical industry. *JACS Au* **2**, 1054–1070 (2022).
26. Digdaya, I. A. et al. A direct coupled electrochemical system for capture and conversion of CO_2 from oceanwater. *Nat. Commun.* **11**, 4412 (2020).
27. Liu, Y., Ye, H.-Z., Diederichsen, K. M., Van Voorhis, T. & Hatton, T. A. Electrochemically mediated carbon dioxide separation with quinone chemistry in salt-concentrated aqueous media. *Nat. Commun.* **11**, 2278 (2020).
28. Rau, G. H., Willauer, H. D. & Ren, Z. J. The global potential for converting renewable electricity to negative-CO_2-emissions hydrogen. *Nat. Clim. Change* **8**, 621–625 (2018).
29. Wang, M., Herzog, H. J. & Hatton, T. A. CO_2 capture using electrochemically mediated amine regeneration. *Ind. Eng. Chem. Res.* **59**, 7087–7096 (2020).
30. Welch, A. J., Dunn, E., DuChene, J. S. & Atwater, H. A. Bicarbonate or carbonate processes for coupling carbon dioxide capture and electrochemical conversion. *ACS Energy Lett.* **5**, 940–945 (2020).
31. Gilliam, R. J. et al. Low voltage electrochemical process for direct carbon dioxide sequestration. *J. Electrochem. Soc.* **159**, B627 (2012).
32. Park, H. S. et al. CO_2 fixation by membrane separated NaCl electrolysis. *Energies* **8**, 8704–8715 (2015).

33. Stucki, S., Schuler, A. & Constantinescu, M. Coupled CO_2 recovery from the atmosphere and water electrolysis: feasibility of a new process for hydrogen storage. *Int. J. Hydrogen Energy* **20**, 653–663 (1995).
34. Rahimi, M. et al. Carbon dioxide capture using an electrochemically driven proton concentration process. *Cell Rep. Phys. Sci* **1**, 100033 (2020).
35. Prajapati, A. et al. Migration-assisted, moisture gradient process for ultrafast, continuous CO_2 capture from dilute sources at ambient conditions. *Energy Environ. Sci.* **15**, 680–692 (2022).
36. Legrand, L., Shu, Q., Tedesco, M., Dykstra, J. & Hamelers, H. Role of ion exchange membranes and capacitive electrodes in membrane capacitive deionization (MCDI) for CO_2 capture. *J. Colloid Interface Sci.* **564**, 478–490 (2020).
37. Willauer, H. D., DiMascio, F., Hardy, D. R. & Williams, F. W. Feasibility of CO_2 extraction from seawater and simultaneous hydrogen gas generation using a novel and robust electrolytic cation exchange module based on continuous electrodeionization technology. *Ind. Eng. Chem. Res.* **53**, 12192–12200 (2014).
38. de Lannoy, C.-F. et al. Indirect ocean capture of atmospheric CO_2: part I. Prototype of a negative emissions technology. *Int. J. Greenh. Gas. Control* **70**, 243–253 (2018).
39. Sharifian, R., Boer, L., Wagterveld, R. & Vermaas, D. Oceanic carbon capture through electrochemically induced in situ carbonate mineralization using bipolar membrane. *Chem. Eng. J.* **438**, 135326 (2022).
40. Mehmood, A. et al. A novel high performance configuration of electrochemical cell to produce alkali for sequestration of carbon dioxide. *Electrochim. Acta* **219**, 655–663 (2016).
41. Xia, C., Xia, Y., Zhu, P., Fan, L. & Wang, H. Direct electrosynthesis of pure aqueous H_2O_2 solutions up to 20% by weight using a solid electrolyte. *Science* **366**, 226–231 (2019).
42. Xia, C. et al. Continuous production of pure liquid fuel solutions via electrocatalytic CO_2 reduction using solid-electrolyte devices. *Nat. Energy* **4**, 776–785 (2019).
43. Kim, J. Y. T. et al. Recovering carbon losses in CO_2 electrolysis using a solid electrolyte reactor. *Nat. Catal.* **5**, 288–299 (2022).
44. Shin, H., Hansen, K. U. & Jiao, F. Techno-economic assessment of low-temperature carbon dioxide electrolysis. *Nat. Sustain.* **4**, 911–919 (2021).
45. *FY 2018 Progress Report for the DOE Hydrogen and Fuel Cells Program* (US Department of Energy, 2019).

Acknowledgements

This work was supported by the Robert A. Welch Foundation (grant number C-2051-20230405) and the David and Lucile Packard Foundation (grant number 2020-71371).

Author contributions

X.Z. and H.W. conceived the project and designed the experiments. X.Z. and Z.F. performed the experimental study. P.Z. performed the TEA study. Y.X. performed the energy consumption comparison of different methods. X.Z. and H.W. wrote the paper with support from all authors. H.W. supervised this project.

Competing interests

X.Z. and H.W. are listed as inventors on a patent application filed by the Rice University that pertains to this work. The other authors declare no competing interests.

Additional information

Supplementary information The online version contains supplementary material available at https://doi.org/10.1038/s41560-024-01654-z.

Correspondence and requests for materials should be addressed to Xiao Zhang or Haotian Wang.

Peer review information *Nature Energy* thanks Ung Lee and the other, anonymous, reviewer(s) for their contribution to the peer review of this work.